M R S Internet Journal Nitride Semiconductor Research

Threshold currents of nitride vertical-cavity surface-emitting lasers with various active regions

Pawe , Ma kowiak[1] and W odzimierz Nakwaski[1]
[1]*Institute of Physics, Technical University of ód ,*

(Received Thursday, June 18, 1998; accepted Wednesday, October 7, 1998)

A detailed threshold analysis of room-temperature pulsed operation of GaN/AlGaN/AlN vertical-cavity surface-emitting lasers (VCSELs) is carried out. The model takes advantage of the latest results concerning gain in active regions, material absorption in the cladding layers, as well as cavity diffraction and scattering losses. The simulation showed that although VCSELs with single (S) or multiple (M) quantum-well (QW) active regions exhibit lower threshold currents, they are much more sensitive to any increase in optical losses than their bulk counterparts. In particular, decreasing the active region radius of gain-guided QW VCSELs below 5 μm (which increases diffraction losses) or increasing dislocation densities (which, in turn, raises scattering losses) gives an enormous rise to their threshold currents. Therefore small-size GaN VCSELs should have an index-guided structure. In the case of MQW VCSELs, the optimal number of quantum wells strongly depends on the reflectivities of resonator mirrors. According to our study, MQW GaN lasers usually require noticeably lower threshold currents compared to SQW lasers. The optimal number of QW active layers is lower in laser structures exhibiting lower optical losses. Although the best result occurred for an active region thickness of 4 nm, threshold currents for the various sizes differ insignificantly.

1 Introduction

Nowadays, ultra-violet (UV) and blue light emitting nitride semiconductor lasers based on wide-gap GaN, AlN, and InN semiconductor materials and their solid solutions [1], are attracting considerable attention. This is due to possibly wide applications of these lasers, especially in high-density optical recording devices [2], and the printing and imaging industry. Recent technology advancements for nitride lasers, achieved primarily by Shuji Nakamura with his co-workers from Nichia Chemical Industries, Ltd., has resulted in immediate progress in laser performance. Only 12 months after the first announcement, at the beginning of 1996 [3], of pulsed operation of nitride lasers at room temperature (RT), the first RT continuous-wave (CW) operation was obtained [4]. Initially, the lifetime of these first RT CW nitride lasers was extremely short, but it was extended to 35 hours by the end of 1996 [5] and a potential 10,000 hours of RT CW operation was reported recently [6], another 12 months later.

The latest Nichia achievements [6] are very promising but a high density of defects in their GaN devices [7] seems to be still an unsolved problem in edge-emitting lasers (EELs). These difficulties might be resolved in nitride vertical-cavity surface-emitting lasers (VCSELs) due to the relatively small volumes of their active regions [8]. Also, the serious difficulties in manufacturing smooth highly-reflective mirrors of EELs may be relatively easy to overcome in VCSELs with semiconducting distributed Bragg reflectors (DBRs). However, there have been only a few successful attempts to fabricate optically pumped VCSELs [9] [10]. The reason for this is probably associated with the very high end losses of VCSELs in comparison to EELs. Nevertheless, because of their unique properties VCSEL structures are unquestionably an inevitable future of nitride lasers. Therefore, an analysis of their RT operation will be helpful in optimization of their possible configurations.

To the authors' best knowledge, the only threshold estimation for RT operation of nitride VCSELs was reported by T. Honda et al. [11]. While their optical gain calculations seem to be very reasonable, their optical loss analysis suffers from many drawbacks and unnecessary assumptions leading to inaccurate and very underestimated threshold current densities. In the present paper, careful threshold analysis is reported for a pulsed RT operation of UV-emitting nitride VCSELs

with bulk, single-quantum-well and multiple-quantum well active regions. The analysis is based on recent experimental and theoretical published results.

2 The Model

The analysis does not include thermal and current-spreading effects, therefore, it is carried out for RT pulsed nitride VCSEL operation of the top-emitting VCSEL structure presented in Figure 1. Current-leakage effects are also neglected in this simulation.

Three types of GaN active regions are taken into consideration:

- bulk GaN active region,
- GaN/$Al_{0.2}Ga_{0.8}N$ single-quantum-well (SQW) active region,
- GaN/$Al_{0.2}Ga_{0.8}N$ multiple-quantum-well (MQW) active region.

GaN active regions (instead of the InGaN active regions usually used in nitride EELs) were chosen intentionally to shift laser emission bands to lower wavelengths, for which material absorption in AlGaN layers is much lower. This kind of absorption may be considerably reduced in nitride EELs where penetration of cladding AlGaN layers by stimulated radiation is limited by their much lower refractive indices. It is, however, unavoidable in nitride VCSELs, in which stimulated radiation is traveling across AlGaN spacers. Both (P-type and N-type) spacers are assumed to be fabricated from $Al_{0.1}Ga_{0.9}N$ and both DBR mirrors - from AlN/$Al_{0.15}Ga_{0.85}N$.

The lasing threshold condition may be written in the following form [12]

$$\Gamma_A \, g_{th} = \alpha_{int} + \alpha_{end} \tag{1}$$

$$\alpha_{int} = \Gamma_A \alpha_A + \Gamma_P \alpha_P + \Gamma_N \alpha_N + \alpha_{diff} + \alpha_{scatt} + \Gamma_M \alpha_M \tag{2}$$

$$\alpha_{end} = \frac{1}{2L} \ln\left(\frac{1}{R_F R_R}\right) \tag{3}$$

where Γ_i and α_i (i = A,P,N) are, respectively, the confinement factors and losses in corresponding layers, L is the resonator length, R_F and R_R are the reflectivities of the front (output) and the rear resonator mirrors, respectively, g_{th} is the threshold optical gain, and Γ_M and α_M will be defined later.

In determining the resonator length L ($L = d_A + d_N + d_P + l_N + l_P$), not only the thicknesses of the active region (d_A) and the *N*-type (d_N) and the *P*-type (d_P) cladding layers should be taken into account, but also the energy penetration depths of the *N*-type (l_N) and the *P*-type (l_P) DBR mirrors. The latter thicknesses can be determined with the aid of the formulae derived by D. I. Babi and S. W. Corzine [13].

Assuming a uniform intensity distribution within the laser resonator, the confinement factors may be easily expressed as

$$\Gamma_i = d_i / L \tag{4}$$

for i = A, P, N respectively. At normal incidence, a periodic structure of quarter-wave-thick layers exhibits the following reflectivity [14]:

$$R = \left[1 - \frac{n_m}{n_1}\left(\frac{n_L}{n_H}\right)^{2m}\right]^2 \Bigg/ \left[1 + \frac{n_m}{n_1}\left(\frac{n_L}{n_H}\right)^{2m}\right]^2 \tag{5}$$

where m is the number of periods in the mirror, n_1 and n_m are the refractive indices of the medium on the transmitted and incident sides of the DBR mirror, and n_L and n_H stand for the refractive indices of alternate sections of the mirror. For the rear *N*-type DBR, the transmitted medium is the substrate, and the incident one is the spacer whereas for the output *P*-type DBR they are the external medium (air) and again the spacer, respectively. Their reflectivities for the rear *N*-type DBR (R_R) and for the output *P*-type DBR (R_F) are directly associated with their numbers (m_R and m_F, respectively) of periods of alternate layers.

Following the approach of D. I. Babi et al. [15], diffraction losses α_{diff} for the UV laser may be found from their Figure 4 with Fresnel number N_F:

$$N_F = r^2_A / \chi_D \tag{6}$$

$$\chi_D = \frac{\lambda_0^2}{4}\left(\frac{1}{n_L^2} + \frac{1}{n_H^2}\right)\frac{n_i}{n_H - n_L} \tag{7}$$

where r_A stands for the active-region radius, λ_0 is the design wavelength and n_i is the refractive index of the spacer. For the laser structure under consideration (c.f. Figure1), diffraction losses were found to be equal to $0.03/L$ for r_A=2.5 μm, $0.016/L$ for r_A = 3 μm, $0.002/L$ for r_A = 5 μm and $0.001/L$ for r_A = 7 μm.

In conventional diode lasers manufactured in both the GaAs/AlGaAs and the InP/InGaAsP systems, material losses in cladding layers may be completely neglected. Optical measurements of nitrides [16] [17] [18] [19] reveal, however, long tails of density of states extending deeply into the band gap. Therefore active-region losses are mainly free-carrier losses:

$$\alpha_A \cong \alpha_{fc,A} \quad (8)$$

whereas optical losses in spacers contain also material losses $\alpha_{m,P}$ and $\alpha_{m,N}$ [20] [21]:

$$\alpha_P = \alpha_{fc,P} + \alpha_{m,P} \quad (9)$$

$$\alpha_N = \alpha_{fc,N} + \alpha_{m,N} \quad (10)$$

In ideal cladding layers, these are negligible, increasing, however, very quickly with deterioration of crystallographic perfection. Unexpectedly high material losses reported for AlGaN layers (see e.g. Figure 2 in [22]) are probably a result of their spatially nonuniform compositions (and maybe also, but to smaller extent, inhomogeneous doping levels). In the model, we also take into account material losses in the DBR mirrors (α_M) within the energy penetration depths (l_N and l_P). Strictly speaking, we assume these losses to be confined to the $Al_{0.15}Ga_{0.85}N$ layers (Γ_M) because of the much wider energy gap of the AlN layers.

For the wavelength of 370 nm and the spacer composition $Al_{0.1}Ga_{0.9}N$, the reported values of material absorption range from 10 cm^{-1} [20] up to as much as 500 cm^{-1} [19] [22]. Free-carrier losses were deduced from Figure 3 in Ref. [23] to be equal to about 1 cm^{-1}.

Light scattering by edge dislocations has been found by L. Liau et al. [24] to be a crucial optical loss mechanism in nitride layers. According to the paper of S. D. Lester et al. [7], spectacular blinding blue LEDs manufactured by Nichia surprisingly contained as many as 10^{10} to 10^{11} dislocations per cm^2. Even for a relatively low dislocation density $N_D = 2 \cdot 10^{10}$ cm^{-2}, scattering losses α_{scatt} as high as 300 cm^{-1} were found [24]. To decrease them to an acceptable range of 5 cm^{-1}, the dislocation density N_D must be reduced to as low as $3 \cdot 10^8$ cm^{-2} [24]. A larger reduction was reported very recently using the lateral epitaxial overgrowth method of growing GaN layers [25]. This technique is expected to lower the dislocation density by at least 3-4 orders of magnitude [26]. If so, then the corresponding scattering losses could be neglected.

Mirror losses α_M are associated with light scattering and absorption within the DBR-mirrors because of imperfections of their structure, including material absorption inside their layers, absorption on layer edges, scattering by material imperfections (e.g. dislocations) and scattering because of non-uniform layer thicknesses. They are difficult to determine, so for simplicity, they were incorporated in the model by assuming scattering (α_{scatt}) and absorption losses ($\alpha_{m,P}$, $\alpha_{m,N}$) within energy penetration depths of both resonator mirrors. It should be remembered, however, that mirror losses start growing quickly after exceeding some number of structure periods, depending on the technology or equipment used. So they ought to be taken into account when optimizing the structure of nitride lasers (c.f. 30-period $Al_{0.4}Ga_{0.6}N/Al_{0.12}Ga_{0.88}N$ Bragg reflectors reported by J. M. Redwing et al. [9]).

The maximum optical gain in a bulk active region may be written as

$$g(n) = a(n - n_{tr}) \quad (11)$$

whereas for a single-quantum-well active region, a logarithmic relation in the following form is often used:

$$g(n) = b \ln(n / n_{tr}) \quad (12)$$

In the above expressions, a is the differential gain, n stands for the carrier concentration, n_{tr} is the transparency concentration, and b is a coefficient directly proportional to a. Following the approach of A. T. Meney and E. P. O'Reilly [27] and T. Honda et al. [11] for the bulk GaN active region, we found: $n_{tr} = 0.75 \cdot 10^{19}$ cm^{-3} and $a = 2.5 \cdot 10^{-16}$ cm^2. Values of analogous parameters for single and multiple GaN quantum well active regions are obtained from data reported in Ref. [28] and are listed in Table 1. The lowest threshold was found for an active region thickness of 4 nm ($n_{tr} = 1.22 \cdot 10^{19}$ cm^{-3} and $b = 6.72 \cdot 10^3$ cm^{-1}).

The threshold carrier density n_{th} may be found from Equation (1) with the threshold gain $g_{th} = g(n = n_{th})$. The threshold current density j_{th} is directly related to n_{th} from the following relation [29]:

$$j_{th} = e d_A (A n_{th} + B n_{th}^2 + C n_{th}^3) \quad (13)$$

where e is the electron charge, A is the monomolecular recombination coefficient (mostly associated with nonradiative recombination at point defects), B is the bimolecular recombination coefficient (principally connected with radiative recombination), and C is the Auger recombination coefficient. In InGaAsP, the A coefficient is in the range of $(1\text{-}2) \cdot 10^8$ s^{-1} at room temperature [30] [31] and is slowly reduced with a decrease in temperature [32], i.e. with an increase in an energy gap. Therefore we assume for GaN $A = 1.0 \cdot 10^8$ s^{-1}. The bimolecular radiative recombination coefficient B for

GaN at room temperature was calculated in Ref. [33] ($B = 0.15 \cdot 10^{10}\ cm^3\ s^{-1}$). Finally, a value for the Auger recombination coefficient $C = 1.4 \cdot 10^{-31}\ cm^6 s^{-1}$ was found using an extrapolation of the dependence of C values of many semiconductor materials on their electron effective masses (see Figure 2). In the above, we assume perfect recombination for carriers above their threshold concentration, according to suggestion of K. Petermann [34].

In case of MQW active layers, homogeneous injection of carriers in all quantum wells is assumed [35] and the cumulative thickness of the active region is just the sum of the thicknesses of all the individual active regions.

Strain-related effects have not been included in the analysis,. They comprise the band-gap engineering and the piezoelectric effect. Because of the hexagonal crystal symmetry of wurtzite nitrides and their small spin-orbit coupling, band-gap engineering methods happen to be much less effective in nitride heterostructure diode lasers than in conventional zincblende heterostructure diode lasers [36] [37]. Under the high-excitation conditions of nitride heterostructure lasers, on the other hand, the piezoelectric field is completely screened by both the doped impurities and the injected carriers [38] [39] [40] [41]. Therefore our above-mentioned assumption seems to be well justified.

3 Results

For the VCSEL structure under consideration, we assume AlN/$Al_{0.15}Ga_{0.85}N$ distributed Bragg reflector (DBR) mirrors. The $Al_{0.15}Ga_{0.85}N$ material was chosen to ensure a high step change in refractive index between alternate layers of the DBR structure while still maintaining negligible absorption material losses [20]. According to references [22] [42] [43] and [36], the index of refraction for AlN was assumed to be n_{AlN} = 2.21. and n_{AlGaN} = 2.5 for the $Al_{0.15}Ga_{0.85}N$. Reflectivities of the front and the rear AlN/$Al_{0.15}Ga_{0.85}N$ DBR mirrors are plotted in Figure 3 versus the number of periods. They seem to be good enough for nitride VCSELs. Unfortunately, AlN layers and even $Al_{0.15}Ga_{0.85}N$ layers are practically insulators [20], and therefore current paths should be designed in these VCSELs not to penetrate the DBR volumes. It may be accomplished with the aid of the lateral current injection [44] [45], which will be discussed in our next paper dealing with a threshold analysis of a possible continuous-wave operation of nitride VCSELs.

The resonator length L (see Equation (3) and Equation (5)) depends on the periods m_R and m_F of both resonator mirrors, which results in an analogous dependence of end and diffraction losses. To simplify our analysis, it is assumed as a rule in all the calculations, that $m_R = m_F + 10$.

The standard GaN VCSEL structure considered in our calculation has parameters listed in Table 2. The infuence of changes in the radius of active region, in the dislocation density and in the reflectivity of resonator mirrors on the threshold currents of VCSELs with bulk, SQW and MQW active regions is shown in Table 3. Both gain-guided (GG) and index-guided (IG) structures have been distinguished for each type of active region. In the case of MQW VCSELs listed in the table, the number of quantum wells is assumed to be equal to 5.

The dependence of the threshold current density on the reflectivity of resonator mirrors for the both GG and IG VCSEL designs are plotted in Figure 4. Threshold current densities of VCSELs with bulk active regions (B-VCSELs) are found to be of the same order and much less sensitive to increases in the end loss (i.e. to decreases in reflectivity of resonator mirrors) than their GG-QW counterparts. Therefore, if there is any problem with manufacturing resonator mirrors of high-reflectivity, VCSELs with bulk GaN active regions turn out to be superior to those with QW active regions. But before we start designing simple double-heterostructure (DH) GaN VCSELs, we should first answer a very fundamental question: what is the dominant intrinsic optical transition in GaN at room temperature? There is some evidence [46], that in a bulk GaN layer, band-to-band transitions are more probable than the exciton transitions. It still needs confirmation, but if we assume the above mechanism of radiative recombination in a bulk GaN active layer, the electron-hole plasma seems to be responsible for gain in B-VCSELs, as in the case of other III-V semiconductor lasers. In QW nitride VCSELs, on the other hand, a dominant recombination process seems to be associated with exciton transitions [17]. According to suggestions of J. I. Pankove [8], this is probably due to relatively small active-region volumes in QW VCSELs, where there is not enough room (on the average) for more than one defect. This is opposite to B-VCSELs, where an electric field following potential fluctuations induced by many defects in much larger active regions can break up electron-hole pairs that form excitons. The picture, however, is still unclear, so there is now an urgent need of additional investigations on this subject. Also a possible large density of nonradiative recombination centers associated with misfit dislocations may be another problem to solve in nitride VCSELs with bulk active regions. Nevertheless, simple, reliable and efficient DH nitride VCSELs, if possible, are very attractive alternative to their QW counterparts.

Thresholds of SQW and MQW GG-VCSELs are extremely sensitive to diffraction losses α_{diff}, as is evident in Table 3. As one can see, a decrease in the active-region radius r_A below 5 μm is followed by a serious increase in α_{diff}, which causes a moderate increase in the threshold of GG B-VCSELs and an enormous increase in the threshold of SQW and MQW GG-VCSELs. To make the analysis more complete, thresholds of IG-VCSELs are also listed in the table. Their index-guided structure is assumed to be perfect, therefore their diffraction losses are completely neglected ($\alpha_{diff} = 0$), considerably reducing their threshold current densities. It is evident from Table 3, that small nitride VCSELs need to have an index-guided structure to lase.

The efficiency of larger VCSELs strongly depends on the uniformity of the current-density distribution within their active regions [47]. The current-spreading effect is neglected in this model; therefore we limit our analysis to active regions with $r_A \leq 5$ μm, for which the above distribution is relatively uniform. Results obtained for $r_A = 7$ μm are shown only for comparison.

Let us examine an influence of additional scattering losses α_{scatt} on thresholds of the same nitride VCSEL designs. As previously, those losses are followed by only some increase in thresholds of B-VCSELs, whereas an analogous increase in thresholds of all QW VCSELs is extremely high. So if we are not able to manufacture nitride layers of sufficiently low dislocation densities, we had better choose a simple DH VCSEL structure than the QW VCSELs. It is worth noticing that only in case of good crystal quality of semiconductor layers, SQW structures can exhibit lower threshold current densities than their MQW counterparts. The importance of the crystal quality of semiconductor layers in producing efficient and reliable nitride VCSELs is also evident from Table 3.

The essential influence of material losses, α_m, resulting from imperfect crystallographic quality in cladding layers is illustrated in Table 3. As one can also see in Figure 5 (note the logarithmic scale on the current density axis), these losses have an extremely large influence on the thresholds of QW VCSELs, again leaving both DH VCSELs much less affected. Hopefully this kind of loss can be reduced relatively easily by moderate improvements in crystallographic uniformity of the bulk cladding layers which may be expected very soon.

Let us consider the influence of spacers on the thresholds of nitride VCSELs. Standard spacers are assumed to be fabricated from $Al_{0.1}Ga_{0.9}N$ and to have thicknesses of 0.5μm. According to our calculations, reducing these thicknesses to only 0.3 μm improves thresholds of B-VCSELs insignificantly, whereas the thresholds of QW GG-VCSELs are reduced to much greater extent: they turn out, once more, to be very sensitive to changes in the optical losses (see Figure 5 and Table 3).

In our previous paper [48], we showed that B-VCSELs with thinner active-regions exhibit distinctly lower threshold current densities, whereas in the case of SQW VCSELs, there is an optimal active-region thickness of 40 Å. The latter result remains valid for MQW VCSELs, although there is smaller difference in the threshold current densities for different active-region thicknesses. Now let us consider the optimal number of quantum wells (M_{opt}) for the best active-region thickness (d_A = 40 Å) in GG MQW lasers. As depicted in Figure 6 for the standard set of parameters, M_{opt} strongly depends on the reflectivities of the resonator mirrors. So, if there is a problem with manufacturing a high-reflectivity resonator mirror, it is suggested to use more than 10 quantum wells. For higher reflectivities, structures with decreasing number of quantum wells seems to be optimal. In case of IG MQW lasers, the results are similar, but for high-reflectivity resonator mirrors the optimal number of quantum wells is reduced to 2. It is also worth mentioning that threshold currents for SQW lasers in high reflectivity range are very close to threshold currents of the best MQW lasers and may be recommended as they can be produced more easily. It should be concluded as a general rule that the less that total optical losses (i.e. end losses plus internal losses) affect the laser radiation within the resonator the smaller the optimal number of QW active layers becomes (from the minimal threshold point of view). This conclusion agrees well with reported results for nitride EELs of Y. C. Yeo et al. [35] and discussion of D. P. Bour et al. [49].

4 Conclusions

A detailed threshold analysis is carried out for nitride VCSELs to examine the usability of this semiconductor laser configuration for future mass applications. The index-guided nitride quantum-well VCSEL structure ensures the best laser performance, as expected, particularly in the case of small-size VCSELs. But surprisingly, gain-guided QW VCSELs are found to exhibit thresholds comparable to much simpler double-heterostructure VCSELs with bulk active regions.

Surprisingly, thresholds of DH nitride VCSELs are much less sensitive to all the optical losses (e.g. diffraction, scattering, absorption, and end losses) than their quantum-well counterparts. Therefore the QW VCSELs need more advanced technology (e.g. to achieve lower dislocation densities and/or higher facet reflectivities) to be superior.

The optimal number of quantum wells in both GG and IG QW VCSEL structures strongly depends on resonator mirror reflectivities and the recommended values for high-reflectivity resonator mirrors are equal to 5 and 1 respectively, whereas for low reflectivities should be more than 10. Generally, the number of quantum wells giving the best threshold performance for nitride VCSELs is proportional to the total optical losses within their resonators.

This work was supported by the Polish State Committee for Scientific Research (KBN), grant No 8-T11B-018-12.

REFERENCES

[1] S. Strite, H. Morkoç, *J. Vac. Sci. Technol. B* ***10*** , 1237-1266 (1992).

[2] B. D. Terris, H. J. Mamin, D. Rugar, *Appl. Phys. Lett.* ***68*** , 141 (1996).

[3] S Nakamura, M Senoh, S Nagahama, N Iwasa, T Yamada, T Matsushita, H Kiyoku, Y Sugimoto, *Jpn. J. Appl. Phys.* ***35*** , L74-L76 (1996).

[4] S. Nakamura, M. Senoh, S. Nagahama, N. Iwasa, T. Yamada, T. Matsushita, Y. Sugimoto, H. Kiyoku, *Appl. Phys. Lett.* ***69*** , 4056-4058 (1996).

[5] Shuji Nakamura , *MRS Internet J. Nitride Semicond. Res.* ***2*** , 5 (1997).

[6] S. Nakamura, M. Senoh, S. Nagahama, N. Iwasa, T. Yamada, T. Matsushita, "InGaN/GaN/AlGaN-Based Laser Diodes with an Estimated Lifetime of 10000 Hours", 10th Annual Meeting of the IEEE Lasers and Electro-Optics Society, LEOS'97, San Francisco, 10-13 Nov. 1997, Paper PD1.1

[7] S. D. Lester , F. A. Ponce , M. G. Craford, D. A. Steigerwald , *Appl. Phys. Lett.* ***66*** , 1249-1251 (1995).

[8] J. I. Pankove, *MRS Internet J. Nitride Semicond. Res.* ***2*** , 19 (1997).

[9] Joan M. Redwing , David A. S. Loeber, Neal G. Anderson , Michael A. Tischler, Jeffrey S. Flynn , *Appl. Phys. Lett.* ***69*** , 1-3 (1996).

[10] M. Asif Khan, S. Krishnankutty, R. A. Skogman, J. N. Kuznia, D. T. Olson , T. George , *Appl. Phys. Lett.* ***65*** , 520-521 (1994).

[11] T Honda, A Katsube, T Sakaguchi, F Koyama, K Iga, *Jpn. J. Appl. Phys.* ***34*** , 3527-3532 (1995).

[12] B. Mroziewicz, M. Bugajski, W. Nakwaski, "Physics of Semiconductor Lasers" (North Holland, Amsterdam 1991). Chapter 4.1.9

[13] D. I. Babic, S. W. Corzine, *IEEE J. Quantum Electron.* ***28*** , 514 (1992).

[14] M. Born, E. Wolf, "Principles of Optics", (Pergamon Press, New York 1993). Sec. 1.6.5

[15] D. I. Babic, Y. Chung, N. Dagli, J. E. Bowers, *IEEE J. Quantum Electron.* ***29*** , 1950 (1993).

[16] G. Yu, G. Wang, H. Ishikawa, M. Umeno, T. Soga, T. Egawa, J. Watanabe, T. Jimbo, *Appl. Phys. Lett.* ***70*** , 3209 (1997).

[17] S. Chichibu, T. Mizutani, T. Shioda, H. Nakanishi, T. Deguchi, T. Azuhata, T. Sota, S. Nakamura, *Appl. Phys. Lett.* ***70*** , 3440-3442 (1997).

[18] A. J. Fischer, W. Shan, J. J. Song, Y. C. Chang, R. Horning, B. Goldenberg, *Appl. Phys. Lett.* ***71*** , 1981 (1997).

[19] V. E. Bougrov, A. S. Zubrilov, *J. Appl. Phys.* ***81*** , 2952 (1997).

[20] S. Yoshida, S. Misawa, S. Gonda, *J. Appl. Phys.* ***53*** , 6844 (1982).

[21] G. Frankowski, F. Steuber, V. Härle, F. Scholz, A. Hangleiter, *Appl. Phys. Lett.* ***68*** , 3746 (1986).

[22] O. Ambacher, M. Arzberger, D. Brunner, H. Angerer, F. Freudenberg, N. Esser, T. Wethkamp, K. Wilmers, W. Richter, M. Stutzmann, *MRS Internet J. Nitride Semicond. Res.* ***2*** , 22 (1997).

[23] J. I. Pankove, S. Bloom, G. Harbeke, *RCA Rev.* ***36*** , 163 (1975).

[24] ZL Liau, RL Aggarwal, PA Maki, RJ Molnar, JN Walpole, RC Williamson, I Melngailis, *Appl. Phys. Lett.* ***69*** , 1665-1667 (1996).

[25] Tsvetanka S. Zheleva, Ok-Hyun Nam, Micheal D. Bremser, Robert F. Davis, *Appl. Phys. Lett.* ***71*** , 2472-2474 (1997).

[26] Hugues Marchand , J.P. Ibbetson, Paul T. Fini , Peter Kozodoy , S. Keller, Steven DenBaars , J. S. Speck, U. K. Mishra, *MRS Internet J. Nitride Semicond. Res.* ***3*** , 3 (1998).

[27] A. T. Meney, E. P. O'Reilly , *Appl. Phys. Lett.* ***67*** , 3013-3015 (1995).

[28] T. Uenoyama, M. Suzuki, *Proc. SPIE* ***2994*** , 94 (1997).

[29] L. A. Coldren, S. W. Corzine, "Diode Lasers and Photonic Integrated Circuits", (J. Wiley & Sons, New York,1995). Chapter 5.2.2

[30] A. Haug, *IEEE J. Quantum Electron.* ***QE-21*** , 716 (1985).

[31] Y. Zou, J. S. Osinski, P. Grodzinski, P. D. Dapkus, W. C. Rideout, W. F. Sharfin, J. Schlafer, F. D. Crawford, *IEEE J. Quantum Electron.* ***29*** , 1565 (1993).

[32] A. P. Mozer, S. Hausser, M. H. Pilkuhn, *IEEE J. Quantum Electron.* ***QE-21*** , 719 (1985).

[33] Alexey V. Dmitriev, Alexander L. Oruzheinikov, *MRS Internet J. Nitride Semicond. Res.* ***1*** , 46 (1996).

[34] K. Petermann "Laser Diode Modulation and Noise",: (Kluver Academic Publishers/KTK Scientific Publishers, Dordrecht/Tokyo , 1991)

[35] YC Yeo, TC Chong, MF Li, WJ Fan, *J. Appl. Phys.* ***84*** , 1813-1819 (98).

[36] M Suzuki, T Uenoyama, *Jpn. J. Appl. Phys.* ***35*** , 1420 (1996).

[37] M. Suzuki, T. Uenoyama, *J. Appl. Phys.* ***80*** , 6868-6874 (1996).

[38] Andreas Hangleiter , Jin Seo Im, H. Kollmer, S. Heppel, J. Off, Ferdinand Scholz, *MRS Internet J. Nitride Semicond. Res.* ***3*** , 15 (1998).

[39] S. Chichibu, D. A. Cohen, M. P. Mack, A. C. Abare, P. Kozodoy, M. Minsky, S. Fleischer, S. Keller, J. E. Bowers, U. K. Mishra, L. A. Coldren, D. R. Clarke, S. P. DenBaars, *Appl. Phys. Lett.* ***73*** , 496 (1998).

[40] Shigefusa Chichibu, Takayuki Sota, Kazumi Wada, Shuji Nakamura, *J. Vac. Sci. Technol. B* ***16*** , 2204-2214 (1998).

[41] K. Domen, A. Kuramata, R. Soejima, K. Horino, S. Kubota, T. Tanahashi, *IEEE J. Selected Topics Quantum Electron.* ***4***, 490 (1998).
[42] J. Pastrnak, L. Roskovcova, *Phys. Stat. Sol.* ***14***, K5 (1966).
[43] H. Morkoc, S. Strite, G. B. Gao, M. E. Lin, B. Sverdlov, M. Burns , *J. Appl. Phys.* ***76***, 1363-1398 (1994).
[44] J. J. Wierer, P. W. Evans, N. Holonyak, D. A. Kellog, *Appl. Phys. Lett.* ***71***, 3468 (1997).
[45] W. Nakwaski, "Some Unsolved Problems Associated with Designing of Nitride Lasers (invited paper)", *Opto-Electron. Rev.* **6**, 93 (1998)
[46] M Smith, JY Lin, HX Jiang, MA Khan, *Appl. Phys. Lett.* ***71***, 635 (1997).
[47] W. Nakwaski, *Appl. Phys. A* ***61***, 123 (1995).
[48] P. Mackowiak, W. Nakwaski, *Electron Tech.* ***30***, 314 (1997).
[49] D. P. Bour, M. Kneissl, L. T. Romano, M. D. McCluskey, C. C. Van deWalle, B. S. Krusor, R. M. Donaldson, J. Walker, C. J. Dunnrowicz, N. M. Johnson, *IEEE J. Selected Topics Quantum Electron.* ***4***, 498 (1998).
[50] Landolt-Börnstein, "Numerical Data and Functional Relationships in Science and Technology, New Series **17***"*, Springer-Verlag, Berlin (1982)

FIGURES

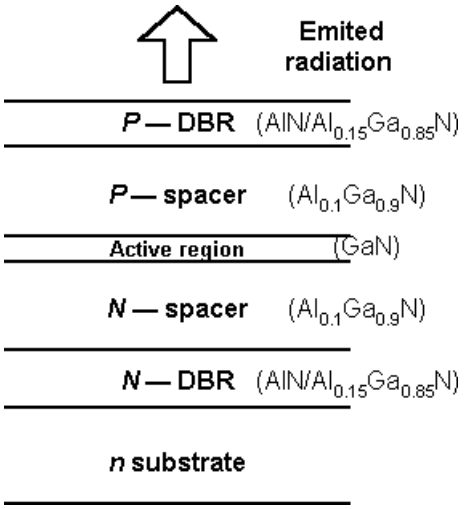

Figure 1. A schematic structure of the considered nitride VCSEL.

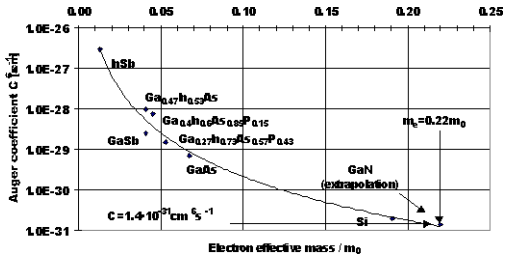

Figure 2. Dependence of the *C* Auger recombination coefficient of many semiconductor materials [50] on their electron effective masses, m_e. The extrapolation giving the *C* value ($C_{GaN} = 1.4 \cdot 10^{-31}$ cm^6s^{-1}) is shown. $m_{e,GaN} = 0.22m_0$ is taken from Ref. [21]. m_0 is the electron rest mass.

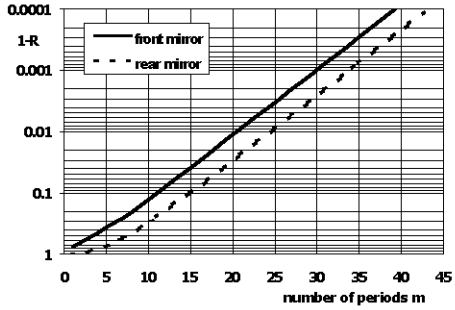

Figure 3. Reflectivity of the front (R_F) and the rear (R_R) AlN/ $Al_{0.15}Ga_{0.85}N$ DBR mirrors versus number *m* of their periods

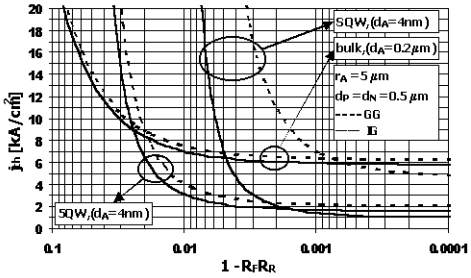

Figure 4. Threshold current density of index-guided (IG) and gain-guided (GG) GaN VCSELs with various active regions versus product of reflectivities of their resonator mirrors.

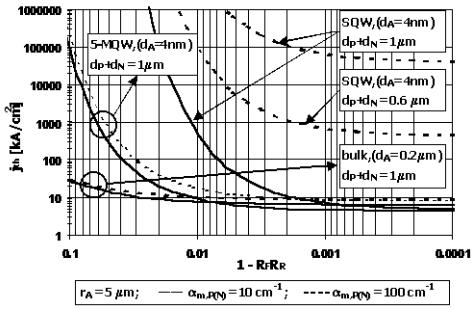

Figure 5. Threshold current density in a logarithmic scale of large (r_A = 5 μm) GaN VCSELs with bulk (d_A = 0.2 μm), SQW or 5-MQW active regions (d_A = 4 nm) of different material losses in cladding layers versus product of reflectivities of their resonator mirrors.

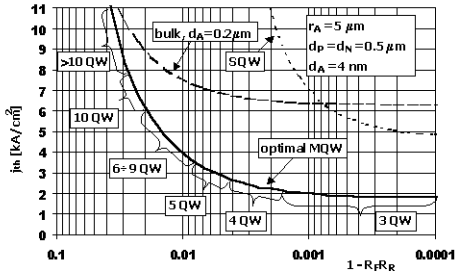

Figure 6. Threshold current density of optimal gain-guided MQW and SQW as well as bulk VCSELs versus product of reflectivities of their resonator mirrors.

MRS Internet J. Nitride Semicond. Res. 3, 35 (1998).

TABLES

Table 1. Gain parameters (averaged over the range $g < 2000$ cm^{-1}) for a single quantum well, extracted from data given in [28].

Quantum-well thickness, Å	n_{tr},10^{19}cm^{-3}	b,10^{3}cm^{-1}
30	1.62	9.05
40	1.22	6.72
50	1.03	5.05
60	0.93	3.99
70	0.87	3.20
80	0.89	3.01

Table 2. Standard set of parameters used to model GaN VCSELs.

Parameter	Symbol	Value
wavelength	λ	370 nm
active-region radius	r_A	5 μm
active-region thickness	d_A	40 D (QW) 0.2 μm (B)
monomolecular recombination	A	$1.0 \cdot 10^{8}$ s^{-1}
bimolecular recombination	B	$1.5 \cdot 10^{-11}$ cm^{3}s^{-1}
Auger recombination	C	$1.4 \cdot 10^{-31}$ cm^{6}s^{-1}
differential gain	a	$2.5 \cdot 10^{-16}$ cm^{2}
gain parameter	b	$6.72 \cdot 10^{3}$ cm^{-1}
transparency concentration	n_{tr}	$1.22 \cdot 10^{19}$ cm^{-3}(QW) $7.5 \cdot 10^{18}$ cm^{-3} (B)
dislocation density	N_D	$3 \cdot 10^{8}$ cm^{-2}
free-carrier losses	α_{fc}	1 cm^{-1}
material losses	α_m	10 cm^{-1}
mirror losses	α_M	10 cm^{-1}
AlN refractive index	n_{AlN}	2.21
GaN refractive index	n_{GaN}	2.74
$Al_{0.1}Ga_{0.9}N$ refractive index	$n_{AlGaN,S}$	2.55
$Al_{0.15}Ga_{0.85}N$ refractive index	$n_{AlGaN,DBR}$	2.5

Table 3. Threshold currents of nitride VCSELs for various active region radius r_A, dislocation density N_D and number of periods of the rear mirror m_R ($m_F = m_R - 10$) for gain-guided (GG) and index guided (IG) laser structures with bulk as well as single (S) and multiple (M) quantum well (QW) active regions ($R_F R_R = 0.999$, except α_{end} part).

		bulk	bulk	SQW	SQW	5-MQW	5-MQW
α_{diff}	r_A	j_{th} (GG)	j_{th} (IG)	j_{th} (GG)	j_{th} (IG)	j_{th} (GG)	j_{th} (IG)
cm^{-1}	µm	kA/cm^2	kA/cm^2	kA/cm^2	kA/cm^2	kA/cm^2	kA/cm^2
5	7	6.2	5.9	3.3	1.5	1.9	1.7
11	5	6.4	5.9	7.7	1.5	2.2	1.7
93	3	10.3	5.9	$1.7 \cdot 10^7$	1.5	18.3	1.7
175	2.5	15.2	5.9	$1.0 \cdot 10^{14}$	1.5	217	1.7
α_{scatt} cm^{-1}	N_D $10^8 cm^2$						
0	0	6.2	5.7	3.8	0.8	2.0	1.5
5	3	6.4	5.9	7.7	1.5	2.2	1.7
30	20	7.6	7.0	425	59.1	4.1	3.0
300	200	28.1	27.0	$4.9 \cdot 10^{24}$	$5.3 \cdot 10^{23}$	$2.5 \cdot 10^4$	$1.6 \cdot 10^4$
α_{end} cm^{-1}	m_R						
1.3	44	6.3	5.8	5.6	1.1	2.1	1.6
3.5	40	6.4	5.9	7.7	1.5	2.2	1.7
15.4	34	6.9	6.4	47.0	7.7	2.9	2.2
32.4	31	7.6	7.1	797	106	4.4	3.31
$\alpha_{m,P}=\alpha_{m,N}$ cm^{-1}	d_P+d_N µm						
0	0.6	6.1	5.6	2.7	0.6	1.9	1.4
10	0.6	6.2	5.8	4.5	0.93	2.0	1.6
100	0.6	7.6	7.1	780	100	4.6	3.4
300	0.6	11.3	10.6	$4.7 \cdot 10^8$	$5.1 \cdot 10^7$	34.0	25.0
500	0.6	16.0	16.0	$3.6 \cdot 10^{14}$	$3.9 \cdot 10^{13}$	350	240
0	1	6.2	5.7	3.3	0.7	1.9	1.5
10	1	6.4	5.9	7.7	1.5	2.2	1.7
100	1	8.8	8.3	$7.3 \cdot 10^4$	8300	8.7	6.4
300	1	16.0	15.0	$4.0 \cdot 10^{14}$	$4.3 \cdot 10^{13}$	320	220
500	1	25.0	24.0	$2.3 \cdot 10^{24}$	$2.5 \cdot 10^{23}$	22000	14000